Earth and Planetary Science Letters 426 (2015) 191–203

Contents lists available at ScienceDirect

Earth and Planetary Science Letters

www.elsevier.com/locate/epsl

Evolution of crustal thickening in the central Andes, Bolivia

Nathan Eichelberger [a,*], Nadine McQuarrie [b], Jamie Ryan [c], Bobak Karimi [b,1], Susan Beck [c], George Zandt [c]

[a] Department of Geosciences, Princeton University, Princeton, NJ 08544, United States
[b] Department of Geology and Planetary Science, University of Pittsburgh, Pittsburgh, PA 15260, United States
[c] Department of Geosciences, University of Arizona, Tucson, AZ 85721, United States

ARTICLE INFO

Article history:
Received 7 March 2015
Received in revised form 18 June 2015
Accepted 21 June 2015
Available online xxxx
Editor: A. Yin

Keywords:
Andean plateau
Altiplano
orocline
shortening
crustal thickness
crustal flow

ABSTRACT

Paleoelevation histories from the central Andes in Bolivia have suggested that the geodynamic evolution of the region has been punctuated by periods of large-scale lithospheric removal that drive rapid increases in elevation at the surface. Here, we evaluate viable times and locations of material loss using a map-view reconstruction of the Bolivian orocline displacement field to forward-model predicted crustal thicknesses. Two volumetric models are presented that test assumed pre-deformation crustal thicknesses of 35 km and 40 km. Both models predict that modern crustal thicknesses were achieved first in the northern Eastern Cordillera (EC) by 30–20 Ma but remained below modern in the southern EC until $\leq$10 Ma. The Altiplano is predicted to have achieved modern crustal thickness after 10 Ma but only with a pre-deformation thickness of 50 km, including 10 km of sediment. At the final stage, the models predict 8–25% regional excess crustal volume compared to modern thickness, largely concentrated in the northern EC. The excess predicted volume from 20 to 0 Ma can be accounted for by: 1) crustal flow to the WC and/or Peru, 2) localized removal of the lower crust, or 3) a combination of the two. Only models with initial crustal thicknesses >35 km predict excess volumes sufficient to account for potential crustal thickness deficits in Peru and allow for lower crustal loss. However, both initial thickness models predict that modern crustal thicknesses were achieved over the same time periods that paleoelevation histories indicate the development of modern elevations. Localized removal of lower crust is only necessary in the northern EC where crustal thickness exceeds modern by 20 Ma, prior to paleoelevation estimates of modern elevations by 15 Ma. In the Altiplano, crustal thicknesses match modern values at 10 Ma and can only exceed modern values by 5 Ma, post-dating when modern elevations were thought to have been established. Collectively, these models predict that the timing of crustal thickening is consistent with paleoelevation data without requiring large-scale removal of lower crust and mantle lithosphere.

1. Introduction

Classically, the topographic growth of compressional mountain belts and associated plateaus has been considered a function of increasing lithospheric thickness in response to orogenic deformation. As shortening accumulates, increasing lithospheric thickness results in the development of isostatically compensated topography. In the central Andes of Bolivia and Peru, the greatest orogen width (~650 km) and highest elevations (~6 km) coincide with the largest shortening magnitudes (~300 km, 40%) and crustal thicknesses (up to 75 km) of the entire chain (Fig. 1), supporting a model of coupled crustal thickening and isostatic elevation gain (e.g. Beck and Zandt, 2002; Isacks, 1988; Kley and Monaldi, 1998; McQuarrie, 2002). Deformation is proposed to have initiated by ~60 Ma along the western margin of the Altiplano, jumping to the eastern plateau margin at the Eastern Cordillera by ~45 Ma and finally to the modern deformation front in the Subandes by ~15 Ma (see Barnes and Ehlers, 2009 and references therein) (Fig. 1). While the protracted nature of upper crustal shortening suggests that modern elevations were achieved gradually, isotopic paleoelevation proxies indicate that elevation gain may have been decoupled from shortening; occurring in rapid, episodic events. Stable isotope data from the Altiplano and Eastern Cordillera argue for elevations <2 km prior to the Miocene, increasing by

* Corresponding author. Present address: StructureSolver LLC, Danville, CA 94526, United States.
E-mail address: nate@structuresolver.com (N. Eichelberger).
[1] Present address: Department of Earth Sciences, Millersville University, Millersville, PA 17551, United States.

http://dx.doi.org/10.1016/j.epsl.2015.06.035
0012-821X/

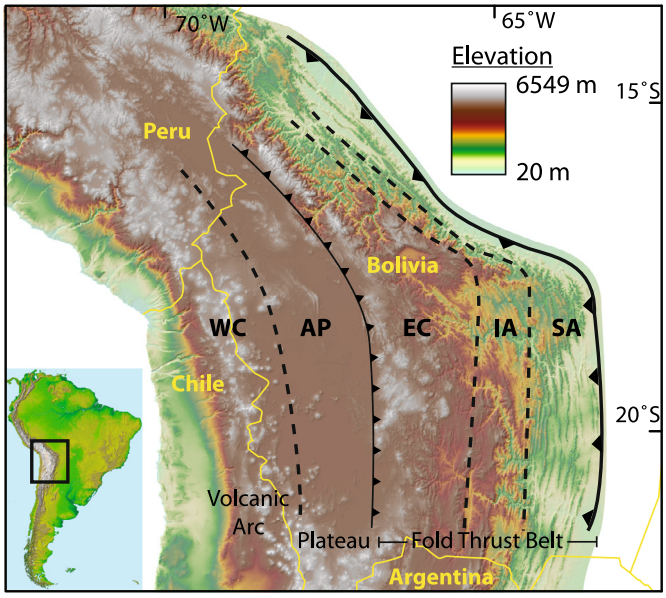

Fig. 1. Shaded digital elevation model of the central Andes. Bold line with teeth represents eastern limit of deformation associated with the Andean fold-thrust belt. Dashed lines delineate the approximate boundaries of the physiographic units present in the study region: Western Cordillera (WC), Altiplano (AP), Eastern Cordillera (EC), Inteandean zone (IA), and Subandes (SA). The EC, IA, and SA are referred to here as the fold-thrust belt as they accommodate the majority of documented crustal shortening at the central Andes. The AP is the internally drained, high elevation basin referred to here as the plateau. The western limit of the plateau is defined by the modern volcanic arc at the WC.

~2.5 km in uplift events at 24–20 Ma in the Eastern Cordillera (Leier et al., 2013) and 10–6 Ma in Altiplano (Garzione et al., 2008; Ghosh et al., 2006). In both cases, the uplift events would have post-dated significant shortening in the region.

Long-term crustal thickening followed by rapid surface uplift in the central Andes is proposed to result from the removal of dense, eclogitic lower crust and underlying mantle lithosphere (Kay and Kay, 1993; Garzione et al., 2008). Alternatively, the gradual development of modern central Andean topography can result from continual, ablative subduction and removal of lithosphere (Tao and O'Connell, 1992; Pope and Willett, 1998) and/or lateral flow and re-distribution of the lower crust (Husson and Sempere, 2003; Yang et al., 2003). Petrologic modeling emphasizes the importance of crustal thicknesses ≥50 km to achieve eclogitic phases from mafic lower crust and the density contrasts necessary to trigger delamination (Kay and Kay, 1993). Lower crustal flow models require thicknesses ≥45–50 km in the Eastern Cordillera to drive flow towards the Altiplano (Husson and Sempere, 2003) and/or along strike to the north and south (Yang et al., 2003). For both mechanisms, understanding when the crust could have reasonably achieved these critical thicknesses is a crucial variable. At a minimum, the magnitude of crustal shortening must account for modern crustal thickness in addition to any crustal material transferred by flow or removed entirely (Beck and Zandt, 2002). Locations where shortening predicts crustal thicknesses greater than modern could indicate areas of material loss while regions with predicted thicknesses below modern could indicate material addition by lower crustal flow. The models presented here do not track thickening of the mantle lithosphere, and require processes such as ablative subduction to prevent large accumulations of mantle lithosphere, even if no excess crust is predicted.

Initial 2-D thickness calculations based on balanced cross sections from the Altiplano-Puna region suggested a 20–30% crustal deficit in Bolivia, and up to 60% in northern Argentina (Kley and Monaldi, 1998). More recent shortening estimates covering the full retro-arc fold-thrust belt width indicate a near balance in Bolivia (e.g. McQuarrie, 2002) but still predict deficits in southern Peru and northern Argentina (Gotberg et al., 2010). A major limitation of 2-D calculations is that the shortening estimates neglect 3-D structural complexities in the orogenic displacement field related to the curvature of the central Andes. These complexities require a 3-D approach to reconcile variations in shortening, paleomagnetic rotations (Arriagada et al., 2006; Roperch et al., 2006), and material displacements parallel to orogenic trend (Kley, 1999; Hindle et al., 2005) to accurately relate Andean deformation to crustal thickening.

An established approach to modeling the evolution of curved mountain belts is to use map-view reconstructions of deformation (e.g. Laubscher, 1965) to determine how the orogenic displacement field affects crustal thickness. Existing 3-D models of the central Andes have demonstrated the importance of material displacement parallel to orogenic trend in calculating crustal thickness (Hindle et al., 2005). As yet, no reconstructions of the central Andes integrate both kinematic and timing data to model the temporal evolution of the crust. Deformation timing constraints are required in order to compare the distribution of crustal thickening predicted by kinematic data to rapid surface uplift events indicated by isotopic data.

Here we present a volumetrically balanced reconstruction of crustal thickening at the Bolivian Andes spanning 50 Ma to present. The model uses the displacement field from reconstructions of the Bolivian orocline (Eichelberger and McQuarrie, 2015) to constrain map-view area change over time. Structurally predicted crustal thicknesses are calculated in 5 Myr intervals by assuming constant volume and a range of pre-deformation crustal thicknesses. At each time step, the predicted crustal thicknesses are compared to the modern crustal thickness distribution determined from broadband seismic data from across the region. By tracking the spatial and temporal evolution of crustal thickness through time, we can identify viable locations and times for lower crustal flow or lithospheric removal.

2. Methods

Modeling the evolution of crustal thickness in response to orogenic deformation requires a kinematic model defined by the 3-D dimensional orogenic displacement field. We utilize the displacement field defined by the map-view fault block reconstruction of Eichelberger and McQuarrie (2015) (Fig. 2). Andean deformation was restored based on available kinematic data by displacing and rotating the faults blocks back to pre-deformation positions. Displacement magnitudes were defined by shortening estimates from balanced cross sections across the retro-arc fold thrust belt in Bolivia (Fig. 2A). The orocline limb rotation magnitudes were set at 13° based on data from regional paleomagnetic rotations (Arriagada et al., 2006; Roperch et al., 2006) and GPS data (Allmendinger et al., 2005). Rotations were applied as a function of cumulative Subandean displacement: blocks near the foreland rotate minimally while blocks at and westward of the western Subandean boundary rotate the full 13°. Strike-slip fault displacements on the Cochabamba and Rio Novillero faults (Dewey and Lamb, 1992; Eichelberger et al., 2013) were also included at the minimum magnitude necessary to obtain a kinematically consistent reconstruction. The reconstruction is subdivided into the established physiographic units present at the Bolivian Andes. From the eastern foreland towards the high plateau they are: the Subandean zone (SA), Interandean zone (IA), Eastern Cordillera (EC), and eastern Altiplano (AP) (Figs. 1, 2). These subdivisions allow for sequential restoration of fold-thrust belt deformation utilizing timing constraints for each zone. Temporal constraints on the reconstruction were interpreted from thermochronologic exhumation ages

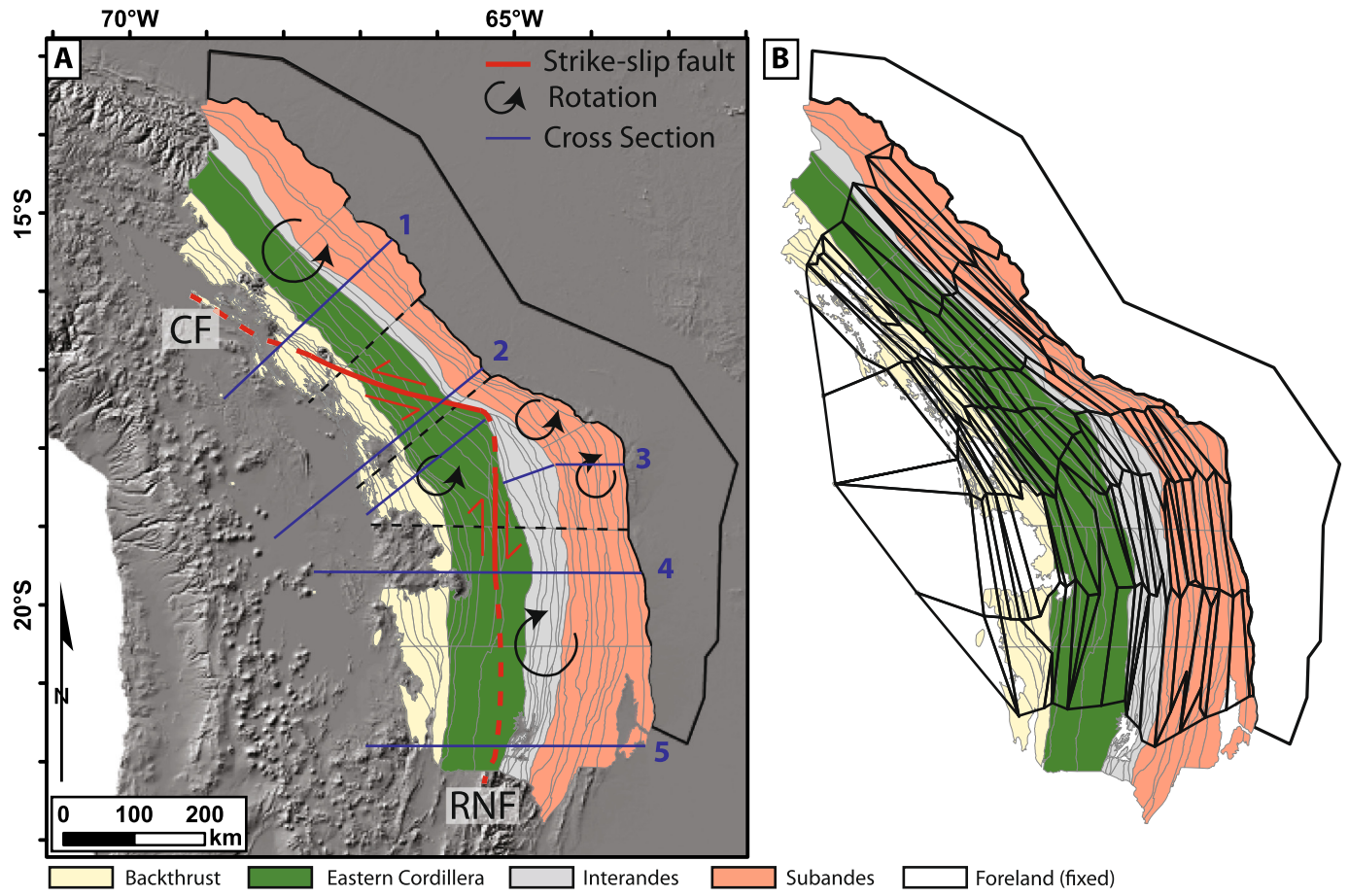

Fig. 2. A) Kinematic model of the Bolivian orocline overlain on GTopo 30 m DEM. The fault blocks are defined by mapped fault and fold traces and grouped by physiographic unit. Dashed lines separate the northern, central, and southern portions of the orocline. The locations of major strike-slip faults included in the model are shown in solid red lines where mapped and dashed elsewhere. The faults included in the displacement field are the Cochabamba Fault (CF) and the Rio Novillero Fault (RNF). Rotations (13°; Eichelberger and McQuarrie, 2015) are also included in the displacement field and the sense of rotation for the northern, central, and southern regions are shown by black arrows. Blue lines indicate location of balanced cross section shortening estimates from 1) McQuarrie et al. (2008), 2) McQuarrie (2002), 3) Eichelberger et al. (2013), 4) McQuarrie (2002), and 5) Dunn et al. (1995), Kley (1996), Müller et al. (2002), Elger et al. (2005). Modified from Eichelberger and McQuarrie (2015). B) Volumetric model mesh. Map-view area change determined by the displacement field is measured by connecting fault block centroids from A into a polygonal mesh. As shortening accumulates from the restored state (50 Ma) to the modern state (0 Ma), the area of the mesh elements contracts. Assuming pure shear deformation, the decrease in area leads to a proportional increase in predicted thickness.

and geologic constraints (references in Eichelberger and McQuarrie, 2015). From this data, deformation in the Bolivian orocline was restored in 5 Myr increments beginning at 50 Ma. The western plateau margin is the modern volcanic arc in the Western Cordillera (WC), but deformation there is not well constrained and omitted from the reconstruction. The modern thickness of the WC is an important parameter that we consider when examining potential crustal redistribution.

The evolution of crustal thickness is estimated from the reconstructed displacement field assuming pure-shear deformation and constant crustal volume through time. The thickness of Andean crust prior to deformation is poorly constrained, so initial crustal thickness is also assumed but varied to determine its influence on the crustal budget and thickening history. Prior 2-D thickness calculations from shortening estimates used a 35–40 km initial thickness range (see references in Gotberg et al., 2010). Broadband seismic data from ~20°S indicate the Brazilian shield is ~30 km thick east of the modern foreland basin (Beck and Zandt, 2002). In the SA, the exposed Paleozoic section ranges from 4 to 8 km thick and increases westward to ~10 km in the southern SA and ~7 km in the northern SA. These Paleozoic rocks are overlain by a thin Mesozoic succession and up to ~3 km of Tertiary foreland basin rocks in the southern SA and ~6 km in the northern SA, suggesting a total thickness of ~10–13 km (Baby et al., 1995; Dunn et al., 1995; McQuarrie, 2002). Given that the modern SA adjacent to the foreland is ~40–45 km thick (including structural shortening), this suggests a possible initial crustal distribution of 25–30 km basement with 10–13 km of sedimentary rocks for an initial crustal thickness range of 35–40 km. In the EC, the Paleozoic section is generally ~10–12 km thick to as high as 15 km (Sempere, 1995; Roeder and Chamberlain, 1995; Welsink et al., 1995). Exposed Tertiary foreland basin sediments in the EC suggest a 3–5 km thick foreland basin once covered the region (e.g. Horton, 2005). Basement thinning toward the west may have accommodated the increase in EC sedimentary thickness over the SA. Based on an initial 35–40 km thick crust, this suggests an EC crust with ~15 km of sediments over a 20–25 km thick basement. Initial crustal thicknesses <30 km are difficult to justify based on the preserved thickness of Paleozoic sediments (10–12 km) and the potential involvement of basement thrusts in Andean deformation that may be up to 15 km thick (e.g. Kley, 1996). To investigate the influence of initial crustal thicknesses on crustal evolution, the volumetric models cover two end-member scenarios: 1) a uniform initial thickness of 35 km and 2) a uniform initial thickness of 40 km. A third model using variable initial thicknesses tapering from 40 km in the SA

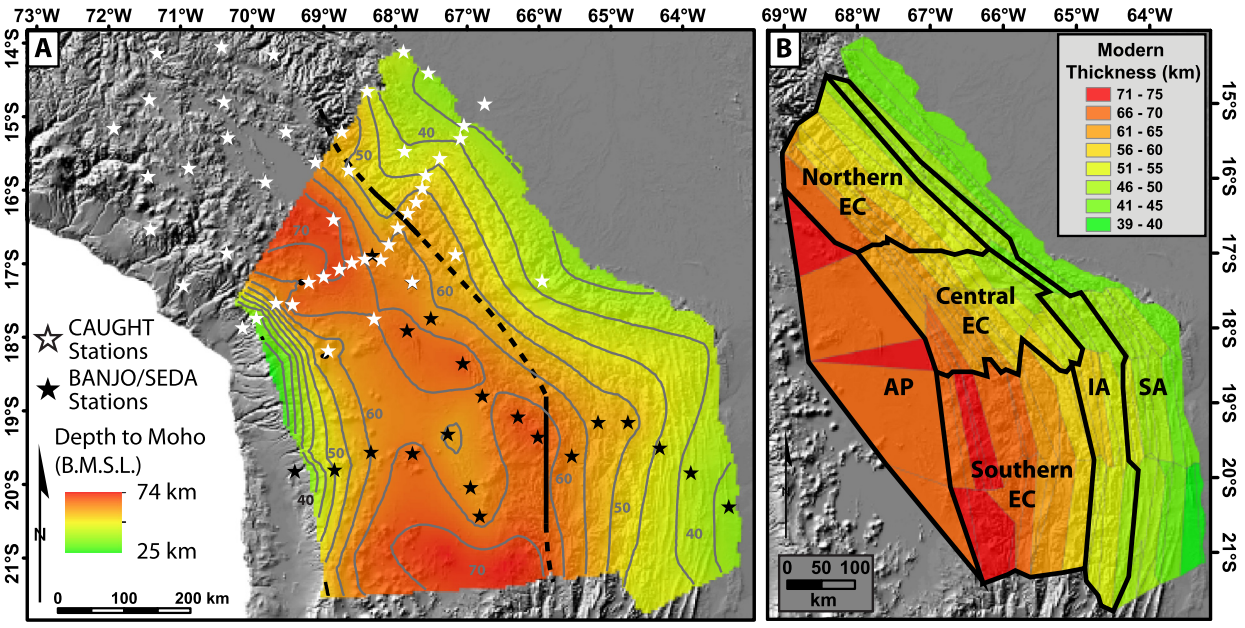

Fig. 3. A) Depth to Moho map (from sea level) for model area from broadband receiver function results from BANJO/SEDA and CAUGHT seismic experiments and gravity data (courtesy of J. Ryan, published in Ryan et al., submitted for publication). Grey solid lines are 5-km contour intervals. Stars represent seismic station locations. The black line indicates the western limit of underthrust Brazilian craton and is solid where constrained by seismic studies (Dorbath et al., 1993; Dorbath and Granet, 1996; Myers et al., 1998) and dashed where interpreted (Beck and Zandt, 2002). B) Volumetric model mesh from Fig. 2B shaded by average thickness. Thickness is calculated by adding Moho depth from A and average elevation. Regions referred to in text are outline in black.

to 30 km at the pre-deformation passive margin at the EC is discussed in Appendix A.

Crustal thickness is calculated based on a pure-shear model using the map-view area change at each time step in the reconstruction. To quantify area, a polygonal mesh was created with nodes defined by the fault block centroids (Fig. 2B). As deformation accumulates forward in time, the distance between the fault blocks decreases. This decreases the distance between mesh nodes and the associated polygonal area between them (Supplemental Fig. S1). The restored, pre-deformation area and the assumed initial crustal thickness define the initial volume for each mesh polygon, which is held constant throughout the model. Predicted crustal thickness is calculated at each time step from the polygon area and volume. These thicknesses are corrected for erosion based on published regional exhumation magnitudes determined from thermochronology (supplemental Fig. S2; see Eichelberger and McQuarrie, 2015 and references therein). Exhumation magnitudes are determined by estimating closure temperature depths using the modern geothermal gradient (e.g. Barnes et al., 2006). Thermochronometers with reset cooling ages (younger than deposition) constrain minimum exhumation magnitudes while un-reset ages (depositional or older) establish the upper limit of exhumation. The correction is applied over the model time periods corresponding to the reported range of cooling ages. To determine when and where predicted crustal thickness exceeds modern values, the model is compared to a modern crustal thickness map based on broadband seismic data, gravity modeling, and modern topography. In the area covered by the model, seismic stations were deployed from 1994 to 1995 as part of the BANJO (Broadband Andean Joint Operation) and SEDA (Seismic Exploration of the Deep Altiplano) experiments (Beck et al., 1994). Combined with seismic data from a deployment completed as part of the Central Andes Uplift and Geodynamics of High Topography (CAUGHT) project (co-authors Ryan, Beck, and Zandt; personal communication) and density modeling of gravity data (Tassara et al., 2006), the modern depth to Moho is fairly well constrained across the model region (Fig. 3A). ASTER 30 m digital elevations models constrained the additional crustal thickness from topography. The sum of the average depth to Moho (below sea level) and elevation (above sea level) were calculated for each polygon element in the volumetric model, giving the modern crustal thickness (Fig. 3B). The predicted crustal thickness for each time step is normalized to the modern thickness, referred to here as the normalized thickness (T_n). In the model, $T_n < 1.0$ indicates a crustal thickness deficit compared to the modern while $T_n > 1.0$ indicates a thickness excess.

Since crustal volume is calculated from reconstructed map-view area change, the principle model uncertainties are associated with the map-view displacement paths (see Eichelberger and McQuarrie, 2015). The fundamental requirement of strain compatibility between balanced shortening estimates, paleomagnetic rotations, and timing data substantially mitigates model errors and yields a best-fit solution but does not quantify variances in modeled area change (McQuarrie and Wernicke, 2005). The map-view displacements used here account for out-of-plane strain, and as a result, exceed plane-strain shortening from balanced cross sections by as much as ~25%. Higher shortening estimates result in greater area change that could bias the models towards excess crustal thickness. To evaluate sensitivity of crustal thickness to shortening estimates, we quantified map-view area change associated with balanced cross section shortening alone. This does not represent a kinematically viable model but provides a low-end assessment of crustal thickening: for a 35 km initial crustal thickness, modern thicknesses are predicted by 0 Ma with no excess material. A complete discussion of this analysis is included in Appendix B.

3. Model results

3.1. Initial model

Applying pure-shear thickening to a uniform initial crustal thickness of 35 km predicts SA and IA crustal thickness up to 5-times greater than modern values (Fig. 4). After the first 5 Myr of SA deformation (15–10 Ma), the predicted thicknesses in the northern SA are within 10% of modern by 10 Ma ($T_n = 0.90–1.10$) whereas the south and central SA average a ~15% deficit ($T_n = 0.75–1.00$). Once SA deformation ceases, the northern SA average

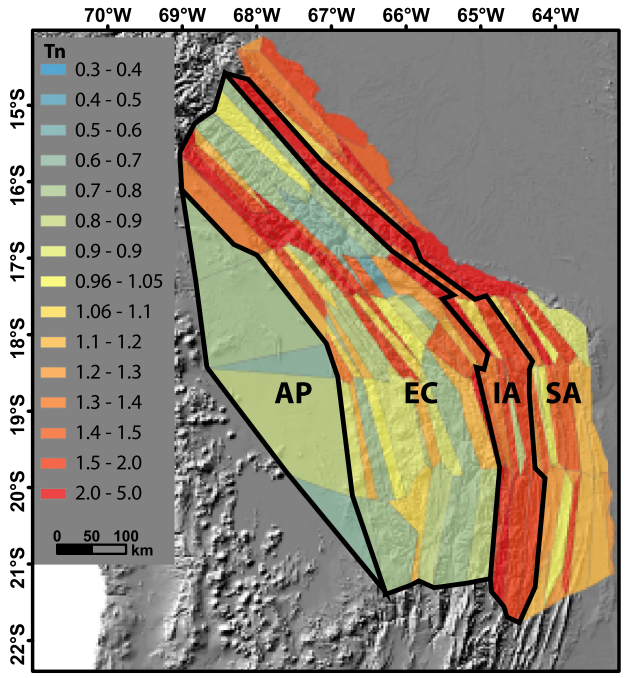

Fig. 4. Initial model results overlain on DEM. Mesh elements are shaded based on pure-shear predicted crustal thickness, represented here by the predicted thickness normalized to the modern thickness (T_n). Physiographic regions are outlined in black. Abbreviations are the same as in the text.

thicknesses are ~60% greater than modern ($T_n = 1.10–2.50$) while the southern SA averages a ~25% excess ($T_n = 0.90–2.10$). In the northern IA, ~10% thickness excesses ($T_n \sim 1.10$) occur as early as 30 Ma. The southern and central IA do not begin to thicken in the model until after 25 Ma with localized excess thickness ($T_n = 1.0–1.40$) predicted by 15 Ma. At 10 Ma the IA is predicted to have regionally exceeded modern thickness by at least 15% ($T_n = 1.15–2.0$). In the northern EC, near-modern to moderate excess thickness is predicted by 30 Ma ($T_n = 0.80–1.20$). By 20 Ma, the model predicts that a swath along the EC–AP boundary would have exceeded modern thickness values by at least 50% ($T_n = 1.5–5$). Conversely, the southern EC maintains deficits to slight excesses ($T_n = 0.7–1.20$) even by the end of southern EC deformation at 20 Ma. The AP never achieves modern thickness, averaging a regional ~30% deficit by 0 Ma ($T_n = 0.65–0.80$).

3.1.1. Initial model implications

As the initial model is parameterized by pure-shear deformation, it demonstrates the effect of local shortening at the fault block scale on crustal thickening. The predicted thickness of a given polygon is a function of shortening accommodated by the fault blocks that define the polygon. This simplification implies that shortening measured at the surface is accommodated by deformation of the entire crustal section. Conceptually, pure-shear thickening requires a weak rheology (England and Houseman, 1988). For the EC and AP at ~20°S, low average crustal seismic velocities are thought to indicate the modern crust is relatively hot (~700–800 °C), dominantly felsic, and lacking a lower mafic component (Beck et al., 1996; Beck and Zandt, 2002; Swenson et al., 2000; Zandt et al., 1996). Based on the crustal composition, likely temperatures, and high surface heat flow, the crust beneath the EC and AP has been interpreted to be weak (Beck and Zandt, 2002). AP and EC topography at 18–20°S appears to be isostatically compensated based on the similarity between geophysically observed and isostatically predicted crustal thickness (Beck et al., 1996; Beck and Zandt, 2002).

On the basis of these observations, the pure-shear lithospheric thickening used in the initial model is most viable for the AP and EC. Conversely, observations for the SA and IA indicate that pure-shear deformation may not be applicable. Seismic data from northern and southern Bolivia indicate that Brazilian lithosphere is intact and underthrust from the foreland to as far west as the lower elevations of the EC (Beck and Zandt, 2002; Dorbath et al., 1993; Myers et al., 1998) (Fig. 3A). The modern crust below the SA and IA is thinner than isostatically predicted, suggesting that they are flexurally supported by the Brazilian lithosphere (Beck et al., 1996), an interpretation also supported by gravity data (Lyon-Caen et al., 1985; Watts et al., 1995; Whitman et al., 1996). Furthermore, reflection seismic data from the SA in Bolivia shows the main decollement depth ranges between 5 and 15 km (Baby et al., 1995; Dunn et al., 1995), implying SA deformation is limited to the upper 15 km of the crust. The extent of the Brazilian lithosphere, as well as the relatively shallow SA detachment, suggests that IA and SA deformation is characterized by brittle deformation on faults that detach above the underthrust Brazilian lithosphere (e.g. Beck and Zandt, 2002). Uniting shallow simple-shear in the IA and SA with pure-shear in the AP and EC to the west implies a transition to ductile deformation distributed throughout the weak EC/AP lithosphere as the Brazilian lithosphere impinges from the east (Beck and Zandt, 2002) (Fig. 5).

3.2. Distributed model

In the initial model, the predicted excess of IA and SA crustal thickness is due to the fact that the starting thickness was only ~5 km below modern, requiring relatively little shortening to exceed modern values. However, as discussed above, IA and SA deformation is limited to the sedimentary section overlying the ~25–30 km thick Brazilian lithosphere (Fig. 5). Therefore, the IA and SA most likely never exceeded their present thickness. As the IA and SA shortened, the rigid Brazilian lithosphere would have been displaced progressively westward into the EC where it is observed today. To reflect this process in the crustal budget, we adapt the initial model to limit predicted crustal thickness in the IA and SA to modern values. The IA and SA progressively thicken during shortening while the volume associated with the basement is displaced westward into the EC and AP. The exact volume of material transferred into the EC and AP depends on the assumed initial crustal thickness, but is volumetrically equivalent to under-thrusting a ~20–30 km thick section of Brazilian lithosphere over the map-view area lost during IA and SA shortening. The volume is transferred across-strike within each region (Fig. 2) first to the EC, followed by the AP. The order is based on the requirement of a crustal thickness gradient between the EC and AP necessary to drive material flow (e.g. Husson and Sempere, 2003; Yang et al., 2003). Predicted EC thicknesses are limited to a maximum of twice the modern thickness ($T_n = 2.0$) so material transferred from the IA and SA is distributed to minimize large thickness gradients within the EC. Within the EC, volume is first added to mesh polygons that are below modern thickness in proportion to area of each mesh polygon. Adding volume based on mesh polygon area limits cases where small polygons rapidly develop extreme crustal thicknesses. Preferentially adding volume to polygons with below modern thickness allows us to recognize areas that develop excess EC crustal thickness prior to IA and SA deformation.

3.2.1. 35 km initial crustal thickness

Since volume transfer to the EC and AP is imposed after the initiation of IA deformation, the distributed and initial models are identical for 50–30 Ma (Fig. 6). As predicted in the initial model, localized excesses ($T_n = 1.2–1.5$) occur along the northern EC–AP by 20 Ma (Figs. 4, 6A). At 15 Ma, the northern EC regionally attains

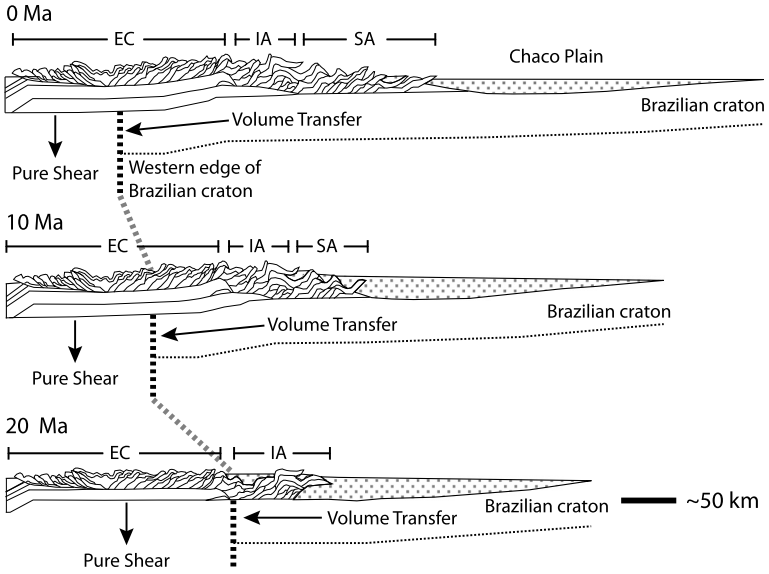

Fig. 5. Schematic reconstruction of the fold-thrust belt at 20 Ma, 10 Ma, and present. At 0 Ma the modern western limit of the Brazilian craton is shown by a vertical, heavy black dashed line. The approximate structural boundaries for each physiographic regions (EC, IA, SA) are shown above the cross sections. The cross sections are fixed in space to show that as east-directed shortening accumulates at the surface, the Brazilian craton is underthrust to the west by an equivalent magnitude. In the distributed volumetric model, this is accounted for by transferring excess volume that would accumulate in the IA and SA westward to the EC. Arrows show the direction of modeled volume transfer from the IA/SA to the EC and additional pure-shear thickening in the EC.

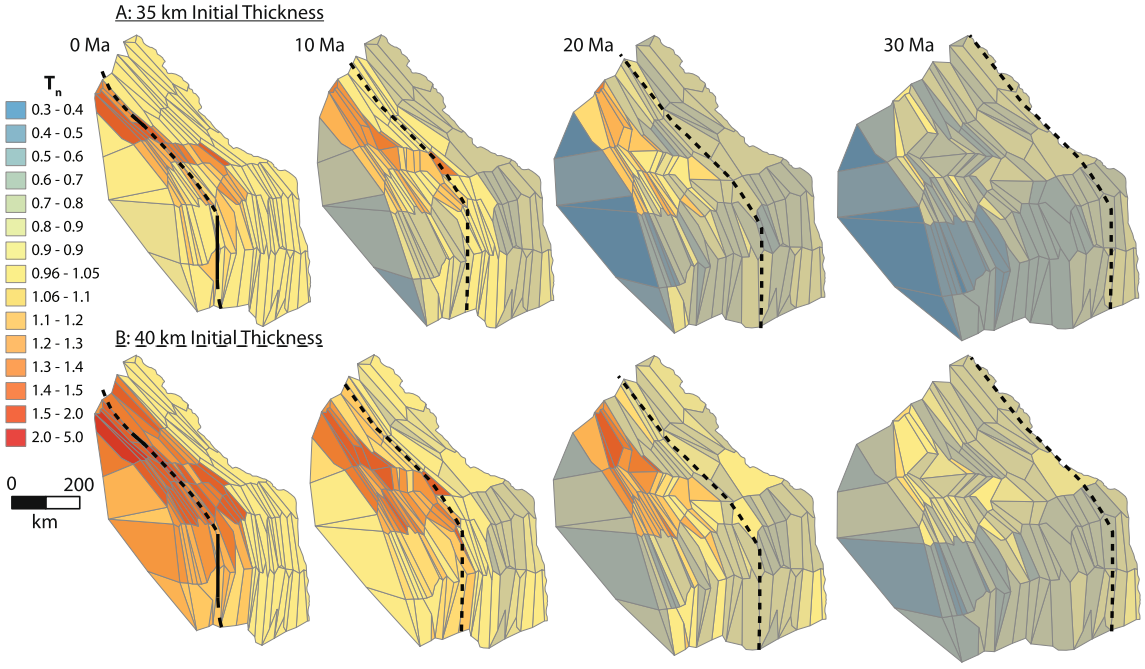

Fig. 6. Uniform initial crustal thickness model results, plotted as crustal thickness normalized to modern (T_n). The black line at 0 Ma shows the modern western limit of the underthrust Brazilian craton (from Beck and Zandt, 2002). From 10 to 30 Ma the approximate restored position is shown by a dashed black line. The 50 km crustal thickness threshold for lower crustal flow (Husson and Sempere, 2003) as well as the eclogite phase transition (Kay and Kay, 1993) occurs at $T_n > 0.7$. A) Uniform 35 km initial crustal thickness model results. B) Uniform 40 km initial crustal thickness model results. Shading and Brazilian craton position is the same as for A.

modern crustal thickness while the western portions of the southern EC are still below modern values. Once SA deformation begins at 10–15 Ma, volume derived from SA shortening and underthrusting of the Brazilian shield is transferred to the AP and EC. This additional volume is distributed across the EC and AP, predicting near modern crustal thicknesses across the entire region by 5 Ma. This model predicts an average 78 ± 30 km ($T_n = 1.4 \pm 0.4$) thick northern EC crust, 72 ± 10 km ($T_n = 1.3 \pm 0.2$) in the central EC, and 70 ± 5 km ($T_n = 1.05 \pm 0.05$) in the southern EC (Fig. 6A). The northern and central AP have final predicted excesses of 10–15%, corresponding to ~10 km of excess crust after 5 Ma. The north–south contrast in predicted EC crustal thickness is due to the fact that the southern EC is nearly double the area of either the central or northern EC, yet it accommodates a similar magnitude of shortening (e.g. McQuarrie, 2002).

Limiting SA and IA crustal thickening to account for a shallow detachment displaced 2.3×10^6 km^3 of material westward over 40–0 Ma. This resulted in substantial thickening in the EC and AP. In the initial model, in situ shortening in the southern EC was insufficient to generate predicted thicknesses near modern. In the

distributed model, the southern EC only exceeds modern thicknesses after 5 Ma once material is transferred from both the IA and SA. In contrast, the northern EC develops excess thickness adjacent to the AP–EC boundary as a result of early in situ shortening (20–25 Ma, Fig. 4) that becomes more widespread when volume is transferred from the IA and SA (Fig. 6A). In situ shortening in the AP was also insufficient to reproduce modern thicknesses (Fig. 4). The majority of the volume transferred from the IA and SA over 20–0 Ma filled deficits in the EC and so the entire AP remained below modern after 5 Ma. Even at this point, the southern AP is predicted to have a ∼10% deficit (Fig. 6A).

While the majority of shortening and related crustal thickening are accommodated in the fold-thrust belt, developing conservative estimates of excess crustal volume requires consideration of the full plateau area. By expanding the model area to the western plateau margin and assuming a 40 km initial thickness for the pre-existing arc, we can assess the contribution of westward crustal flow from the retro-arc to fore-arc. The transferred excess would correspond to an additional ∼15 km thickness per unit area, predicting a 55 km thick crust, ∼10 km below the modern mean thickness of 65 km. If the remaining ∼10 km is the result of magmatic addition it would correspond to ∼15% of the total WC volume.

3.2.2. 40 km initial crustal thickness

With the exception of the northern EC, the uniform 35 km thickness model only predicts near modern thicknesses to slight deficits in the EC and AP by 0 Ma. These predictions indicate that assuming initial thicknesses less than 35 km will result in greater deficits for the southern EC and AP area. The 40 km thickness model uses the upper end of plausible pre-deformation crustal thickness to provide an upper limit for the crustal volume budget. Theoretically, this represents the maximum excess crustal volume available for re-distribution and/or removal. To evaluate the limits of material deficits predicted for the AP in the models presented above, AP pre-deformation thickness is increased to 50 km (accounts for ∼10 km of Tertiary sedimentation; e.g. Horton, 2005). In the IA and SA, the initial 40 km model thickness is significantly closer to modern thicknesses (∼40–55 km, Fig. 3). As a consequence, 17% more material (2.7×10^6 km^3 total) is transferred to the EC and AP during SA and IA deformation than in the 35 km initial thickness model.

In the northern EC, the 40 km thickness model predicts modern to near-modern crustal thicknesses by 30 Ma compared to 25 Ma in the 35 km initial thickness model (Fig. 6B). By 20 Ma, 10–50% thickness excesses are predicted across the northern and central EC while the southern EC is dominated by a material deficit (mean $T_n = 0.85 \pm 0.15$). Despite allowing for greater initial thicknesses, in-situ shortening in the AP and southern EC is still insufficient to reproduce modern crustal thicknesses. Both regions require model-imposed volume transfer from the IA and SA to reach modern values and even then, do not uniformly meet or exceed modern thickness until 10 Ma (Fig. 6B). However, due to the greater initial AP thickness (50 km vs. 35 km) and greater volume transfer (2.7×10^6 km^3 vs. 2.3×10^6 km^3) from the IA and SA, the AP is predicted here to have exceeded modern thickness by 5 Ma ($T_n = 1.1$–1.2). This is in contrast to the 35 km thickness model which predicts only modern AP thicknesses by 0 Ma (Fig. 6A).

The total excess volume predicted by the 40 km thickness model at 0 Ma is sufficient to account for the modern thickness of the western plateau margin. Distributing the entire excess over the WC corresponds to an additional 50 km thickness per unit area. Given the assumptions used above (40 km initial arc thickness, negligible magmatic addition), this could easily account for the modern 65 km arc thickness. The remaining excess volume after accounting for the full WC thickness would correspond to an additional 10 km of crust over the entire AP and EC within the model area.

4. Volumetric model implications

Relative to the modern crustal structure, the models presented here predict regional volumetric excess of 8% for a 35 km thick initial crust, 25% excess for 40 km initial thickness, and 5% for a variable thickness crust (Appendix A). The variable thickness model predicted minor excess volume so we focus discussion on the 35 km and 40 km uniform thickness models. The 35 km thickness model results are similar to volumetric predictions made by prior 3-D models (9%; Hindle et al., 2005). However, these studies used a uniform initial thickness of 40 km and shortening magnitudes <250 km (e.g. Kley and Monaldi, 1998). The shortening magnitudes used here exceed 300 km (e.g. McQuarrie, 2002) and as a result, the 40 km initial thickness model predicts twice the excess volume of prior models. Additionally, the modern crustal thicknesses reference used in Hindle et al. (2005) were defined by discontinuous receiver function data (Yuan et al., 2002) and by assuming an elevation–thickness relationship. This may have resulted in over-estimating modern crustal thickness in areas such as the northern EC where recent seismic data shows relatively shallow Moho below regions of high topography (Fig. 3).

Assuming the range of initial crustal thicknesses tested here are correct, the predicted crustal volume excess indicates that lower crustal flow and/or removal of lower crust may have occurred during Andean deformation. Determining the relative importance of lower crustal flow versus wholesale removal requires assessing the possible magnitude of regional crustal flow and considering the timing of crustal thickening with respect to paleoelevation data.

4.1. Lower crustal flow

Based on the predicted magnitude and timing of excess crustal volume, lower crustal flow may have begun as early as 30 Ma near the northern EC and continued through SA deformation (Fig. 6). Gravity driven channel flow models (Poiseuille flow) have simulated AP uplift over the last 20–10 Myr by assuming a 15 km thick channel with viscosities ranging from 2.4×10^{18}–10^{20} Pa s (Husson and Sempere, 2003; Yang et al., 2003). The critical crustal thickness (>50 km) proposed in Husson and Sempere (2003) to produce a low-viscosity channel is predicted here for the northern EC by 25 Ma in the 35 km initial thickness model and 30 Ma in the 40 km thickness model (Fig. 6). Using a 2.4×10^{18} Pa s viscosity (after Husson and Sempere, 2003), mid-crustal density of 2800 kg m^{-3} and the reconstructed distance between the EC and WC at 20 Ma (240 km, 40 km of AP shortening plus the ∼200 km modern AP width), predicts a mean channel flow of ∼100 km Myr^{-1} (Turcotte and Schubert, 2002). Higher viscosities (10^{20} Pa s after Yang et al., 2003) result in a much lower rate of 10 km Myr^{-1}. At ∼100 km Myr^{-1}, material could flow across strike from the EC and reach the WC in ∼2 Myr after the pressure gradient was established. If 10 km Myr^{-1} is used, ∼25 Myr is required. Since the calculation here assumes the pressure gradient is constant, velocity could change with time as crust accumulates or is removed from the system.

Regional crustal flow from Bolivia to Peru has been proposed as a mechanism to account for a ∼20–50 km thickness deficit between shortening and isostatic thickness predictions in the Peruvian AP and WC (Gotberg et al., 2010). Given the ∼350 km along-strike distance between the region where the crust first exceeds 50 km in the northern EC and the Gotberg et al. (2010) study area, a low channel viscosity (∼10^{18}; Husson and Sempere, 2003) is required for any material to reach the northern Peruvian AP by 0 Ma. For a regional 35 km initial crustal thickness, the modern deficit

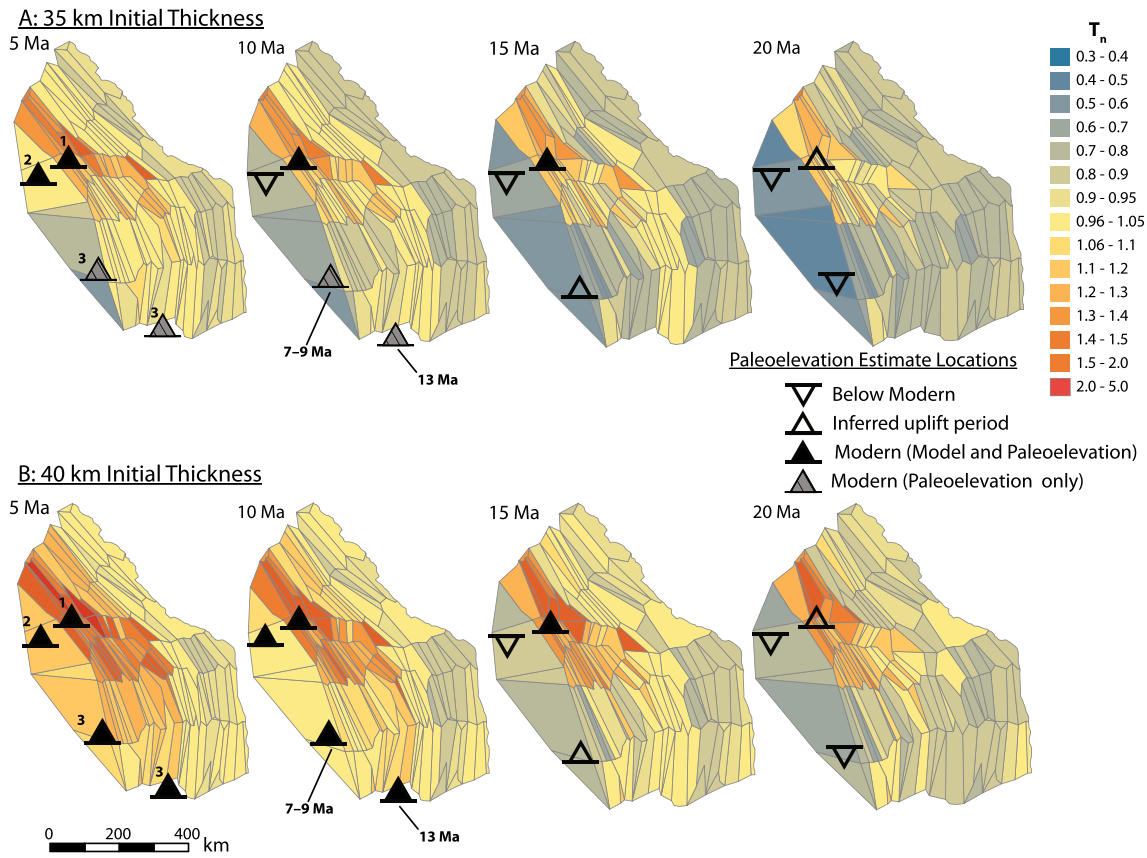

Fig. 7. Volumetric model thickness predictions compared to locations of potential surface uplift. Predicted thicknesses are shown for A) uniform 35 km initial crustal thickness and B) variable initial crustal thickness. Symbols indicate restored locations and times where stable isotope data indicate changes in surface elevation: 1) ~1–2.5 km of EC elevation gain between 25 and 15 Ma (Leier et al., 2013); 2) 1.2–2.6 km of AP elevation gain from 16 to 13 Ma and 0.1–1.3 km from 13 to 9 Ma (Garzione et al., 2014); 3) ~1–2.5 km of AP elevation grain from 10 to 6 Ma (Ghosh et al., 2006; Garzione et al., 2006, 2008).

in Peru is predicted to be 1.9×10^6 km^3 (123 km of shortening in the EC through SA; Gotberg et al., 2010), 45% greater than the 1.3×10^6 km^3 volume excess predicted for the same initial thickness in Bolivia. Transferring the entire excess volume from Bolivia to Peru would require ~10% magmatic addition in the Peruvian AP and EC to account for the remaining 0.6×10^6 km^3 deficit (assuming no internal shortening). In this case, ~45% magmatic addition would be necessary in Bolivia to account for the modern WC thickness (assuming no internal shortening and allowing for an initial 35 km crust). Evenly distributing the excess volume between Peru and Bolivia requires 35% magmatic addition in Bolivia and 25% in Peru. Increasing regional initial crustal thickness to 40 km predicts a deficit of 0.9×10^6 km^3 in Peru while the total excess predicted for Bolivia is 4.8×10^6 km^3, leaving 3.9×10^6 km^3 of material after fully accounting for the modern plateau volume in Peru. Distributing the remaining excess volume over the WC in Bolivia corresponds to 40 km of crust per unit area or ~60% of the 65 km average modern WC thickness. Assuming an initial thickness of 40 km, the total predicted WC thickness would be 80 km. This is 15 km greater than the average modern WC thickness and is equivalent to a final excess volume of 1.5×10^6 km^3. Only models with regional initial thicknesses >35 km have sufficient volume to account for the modern plateau thickness and still allow for loss of lower crust within the AP (volumes from the variable thickness model are insufficient, see Appendix A).

4.2. Removal of lower crust

Within the model area, paleoelevation studies have interpreted punctuated increases in surface elevation at 24–15 Ma in the northern EC (Leier et al., 2013); 16–13 Ma and 13–9 Ma in the southern EC and AP (Garzione et al., 2014); and 10–6 Ma in the northern AP (Garzione et al., 2006, 2008; Ghosh et al., 2006) to indicate removal of the lower crust and mantle lithosphere (Figs. 7, 8). Basalts in southern and central Bolivia (17°–22°S) span 25–0 Ma and are petrologically consistent with shallow mantle melting and relatively thin lithosphere (<100 km) in the region since 25 Ma (Lamb and Hoke, 1997). Within the northern EC, a seismically imaged 5–10 km decrease in Moho depth over an 8700 km^2 area may be further evidence for localized lower crustal loss (Fig. 3).

For the northern EC, both the 35 km and 40 km initial thickness models predict near to greater than modern average crustal thicknesses by ~20 Ma with >40% excess by 0 Ma (Figs. 7, 8A). Crustal thicknesses in the eastern EC only exceed modern values after 15 Ma while the western boundary exceeds modern values by 20 Ma (Fig. 7). The western EC excess is spatially and temporally coincident (Fig. 7) with the 24–15 Ma decrease in paleosurface temperatures recorded by Leier et al. (2013) (Fig. 8A). The timing of surface uplift and presence of excess crust indicate that localized removal of lower crust is possible. At 25 Ma, paleoaltimetry indicates western EC elevations were ≤1/2 modern (Leier et al., 2013) while crustal thicknesses in the area are predicted to be near to greater than modern (Fig. 8A). Maintaining low elevations and a relatively thick crust at 25 Ma requires negatively buoyant material in the lower crust. If the seismically imaged Moho deviation is assumed to approximate the area of removed lower crust, the 20–15 Ma local volume excess from both initial crustal thickness models can support crustal losses equivalent to 10 km from below the northern EC.

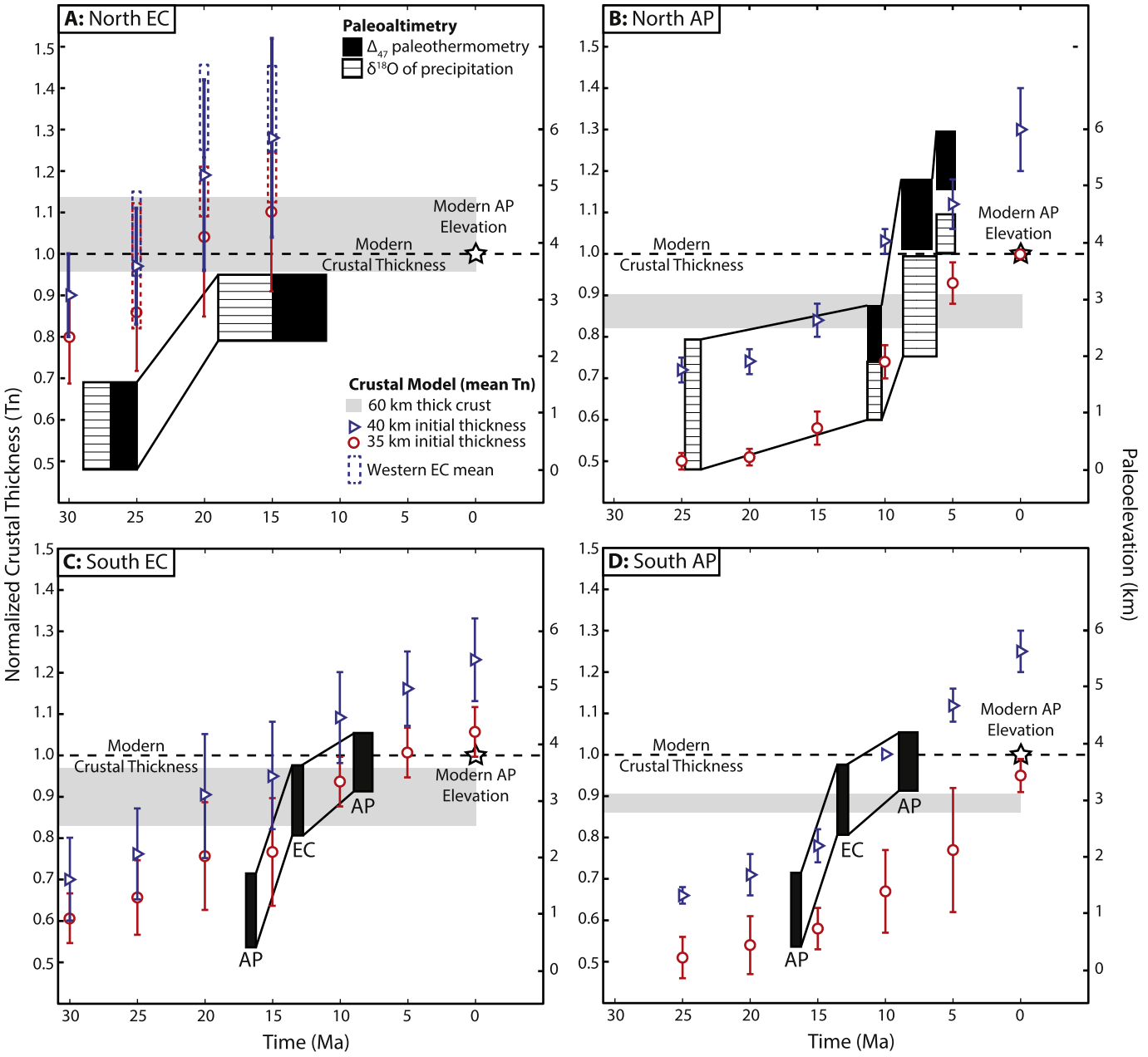

Fig. 8. Timing comparison of predicted crustal thickening (circles, triangles) and paleoaltimetry data (shaded boxes) by region. The left hand vertical axes are normalized crust thickness (T_n) and the right hand vertical axes are elevation. The axes are scaled so modern crustal thickness ($T_n = 1.0$) and mean modern AP elevation (~3.8 km) are collinear (dashed line). Shaded horizontal bars show the range of normalized thicknesses that correspond to a 60 km crustal thickness across each zone. The mean and standard deviations for the normalized crustal thicknesses (T_n) are calculated based on the model extent of each physiographic zone. The spatial variability of normalized thicknesses is shown in Fig. 7. A) Northern EC; large standard deviations in T_n are due to concentration of excess thickness along the western edge of the EC, spatially coincident with paleoaltimetry data (Leier et al., 2013; Fig. 7), dashed boxes refer to T_n range for this area. B) Northern AP; modern crustal thickness is predicted between 10 and 5 Ma and uplift period from paleoaltimetry is 10–6 Ma (Garzione et al., 2008). C) Southern EC; near modern crustal thickness is predicted by 15–10 Ma and paleoaltimetry slightly lower-than-modern elevations by ~13 Ma (Garzione et al., 2014). D) Southern AP; modern crustal thickness predicted by 10 Ma (40 km thickness model only) and paleoaltimetry indicated modern elevations at ~8 Ma (Garzione et al., 2014).

In contrast to the northern EC, the northern AP does not exceed modern crustal thickness until after the 10–6 Ma surface uplift predicted from paleoaltimetry (Garzione et al., 2008) (Fig. 8B). This implies that any hypothetical volume of crust removed to explain abrupt increases in surface elevation would have been initially sourced from the adjacent EC (Fig. 7). Most importantly, both paleoaltimetry and crustal thickness models predict modern values between 10 and 5 Ma, indicating that lower crustal loss is not required to explain the northern AP uplift signal (Fig. 8B). Only the 40 km initial thickness model predicts excess crust after 10 Ma. The excess could be accounted for by removal of the lower crust, but the majority of crustal excess does not accumulate until 5 Ma or later, conflicting with the timing proposed for rapid elevation gain (Fig. 8B). Gradual lower crustal flow is an equally plausible mechanism to explain crustal excess as the conditions necessary for flow existed prior to 10 Ma (Fig. 7) and there is currently no data to support rapid surface uplift younger than 5 Ma.

The timing of crustal thickening in the southern EC and AP are consistent with paleoelevation histories (Figs. 8C, 8D). In the southern EC, average crustal thickness is predicted to be within ~20% of modern during the 15–10 Ma period when paleoelevations were apparently increasing from slightly below modern to

modern elevations (Garzione et al., 2014) (Fig. 8C). For the southern AP, crustal thicknesses between 20 and 15 Ma are predicted to be <80% modern and overlap with predicted paleoelevations of 50–70% of modern (<2 km, Garzione et al., 2014) (Fig. 8D). By 10 Ma both the 40 km thickness model and paleoelevation data indicate modern values, so removal of lower crust is not required to explain increasing surface elevations. After 10 Ma, excess crustal material is predicted for the EC and AP (40 km thickness model only; Figs. 8C, 8D). This post-dates the crustal loss events previously proposed to explain increases in surface elevation (Garzione et al., 2014; Hoke and Garzione, 2008).

At the plateau scale, elevated paleosurfaces and AP isotopic paleoelevation data have been used to argue for regional lithospheric removal from the EC and eastern AP at 10–6 Ma (Hoke and Garzione, 2008). Flexural elevation models predict that removing >10 km of dense lower crust from below the EC and eastern AP is necessary to reproduce a ∼2.5 km paleoelevation increase at 10–5 Ma (Garzione et al., 2008; Hoke and Garzione, 2008) (Fig. 8B). Transfer of material associated with SA shortening to the AP and the concomitant recent uplift was proposed initially in a 2-D model as a way of reconciling shortening and paleoelevation data without the requiring delamination induced uplift (Lamb, 2011). Here, it is shown in 3-D as a mechanism to address the north to south variation in age of uplift as predicted from paleoelevation proxies (Garzione et al., 2014). Although the results here match the timing of elevation gain, the rate of elevation gain is more nebulous. Timing constraints from thermochronology only resolve broad periods of deformation, modeled here in 5 Myr increments. Conversely, paleoaltimetry time constraints are much more precise and cover time intervals <5 Myr. Paleoaltimetry uplift rates appear faster than the modeled rates of crustal thickening but if the model results (Fig. 8) are viewed as end-members, an intermediate crustal thickness (e.g. 37 km) the rate of crustal thickening could be similar.

For initial crustal thicknesses under 40 km, regional material loss is only volumetrically possible if crustal flow from the model area is negligible and WC thickness is internally accounted for (e.g. magmatic addition, local shortening). When distributed over the EC and AP, the total excess volume from the 35 km initial thickness model yields 5 km of excess crust per unit area by 0 Ma. Conversely, the total excess volume from the 40 km initial crustal thickness model corresponds to 10 km of excess crust at 10 Ma and 17 km by 5 Ma. Thus, regional removal of >10 km of lower crust to drive plateau uplift at 10–5 Ma requires initial crustal thicknesses ≥40 km.

5. Conclusions

Overall, the displacement field at the Bolivian Andes predicts greater crustal thicknesses than measured by geophysical data. For pre-deformation crustal thicknesses ≥35 km, modern thicknesses would have been achieved first in the northern EC by 30–25 Ma, across the entire EC by 10–5 Ma, and across most of the AP by 10–0 Ma. The final excess volume depends on assumed initial crustal thickness, but models using variable (30–40 km) and uniform initial thicknesses (35, 40 km) predict final crustal volumes 5–25% greater than modern. With the shortening magnitudes used here, the 35 km initial thickness model generally provides a better fit to the modern crust than the 40 km model. If initial thicknesses were ≥35 km, removal of material is required to achieve balance with modern values.

The two primary mechanisms that account for the excess volume are lower crustal flow and/or removal of dense lower crust. Lower crustal flow to the northern portion of the plateau in Peru may explain the difference between crustal thicknesses predicted by crustal shortening and modern values. Here, only the 40 km initial crustal thickness model predicts sufficient excess volume to account for the deficit in Peru and still accommodate lower crustal removal in Bolivia. An important outcome is models with initial thicknesses ≥35 km predict modern crustal thicknesses over the same time periods (6–10 Ma) that stable isotope data indicate modern surface elevations. As a consequence, lower crustal loss is not required to explain the paleoelevation history recorded in the Altiplano. Although removal of ∼10 km of dense lower crust from below the EC and eastern AP at ∼10 Ma is permissible with an initial crustal thickness of 40 km, removal of negatively buoyant lower crust is only required in the northern EC where crustal thicknesses are predicted to have exceeded modern values (∼20 Ma) before modern elevations were obtained. Elsewhere, excess crustal material only accumulates after modern elevations were achieved, suggesting that the remaining excess volume can be explained by lower crustal flow to the WC and along strike to Peru.

Acknowledgements

The models presented here were developed as part of the NSF funded Central Andean Uplift and Geodynamics of High Topography (CAUGHT) project (EAR# 0908972 to McQuarrie). The initial concept for the paper benefitted from discussions held at annual CAUGHT workshops among the authors with additional input from CAUGHT co-principal investigators Todd Ehlers, Carmala Garzione, Brian Horton, Chris Poulsen, Laura Wagner, and their respective students. Externally, Sean Willett, Blair Schoene, and Adam Maloof also provided insightful comments at early stages that improved the model and presentation of the results. Reviews from Alex Webb and Jonas Kley greatly improved the discussion of model uncertainties and results.

Appendix A

A.1. Variable initial crustal thickness model

Both previously published (e.g. Hindle et al., 2005) models and those presented here assume uniform initial thicknesses. The prediction of excess material in the northern EC and near deficits in the AP and southern EC could be the result of over- or underestimating initial crustal thickness. For the EC to accumulate the 10–15 km Paleozoic marine sediments observed today (Sempere, 1995; Roeder and Chamberlain, 1995; Welsink et al., 1995), the initial EC thickness (including the Paleozoic section) would have been no thicker than the modern craton (30 km, Beck and Zandt, 2002). Decreasing the initial EC crustal thickness to 30 km could reduce the magnitude of excess predicted crust but would not change the relative north–south distribution of shortened crust. Syn-orogenic sedimentation in the AP and SA also argues for variable initial crustal thicknesses. To test this possibility, we modeled crustal thickening using variable initial thicknesses across the model area.

If an initial thickness of 30 km is used as a base-line, accounting for ∼10 km of AP sediment accumulation from pre- to post-EC deformation (50–20 Ma) would increase the initial AP thickness to 40 km and could result in predicted thicknesses closer to modern. Similarly, the SA in the model region has accumulated ∼3–6 km of Tertiary syn-orogenic sediment. Increasing pre-deformation SA thickness would ultimately result in initial thicknesses closer to modern (∼40 km, Fig. 3) and greater volume transfer to the EC and AP. To determine how variable initial thickness influences structurally predicted thicknesses, the variable thickness model utilizes a 30 km initial thickness in the EC and AP and 35 km in the IA and SA. Syn-orogenic sedimentation is accounted for by adding 3–5 km of sediment to the entire AP prior to EC deformation plus an additional 5–7 km from 45 to 20 Ma during EC deformation. In the

SA, 3–6 km of sediment is added from 40 to 15 Ma during IA deformation. By the time deformation begins in the AP and SA, the initial thickness is 40 km.

A.2. Variable initial thickness model results

Reducing the initial thickness of the EC delays the development of modern thickness at any location until the end of EC deformation at 20 Ma compared to 30 Ma in the uniform thickness models (Fig. 6). Even at 20 Ma, only the northern and central EC adjacent to the AP were predicted to have thicknesses within at least 10% of modern. The northern EC near the AP is characterized by ~5–10% excess thickness compared to >20% excess at the same time and location in the uniform thickness models (Fig. 6). Regionally, deficits remain in the EC until 5 Ma whereas the EC in the uniform thickness models attained $T_n > 1.0$ by 15 Ma in the north and central regions and 5 Ma in the south. The average final thicknesses predicted by the variable initial crust model in the EC are 72 ± 20 km ($T_n = 1.25 \pm 0.3$) in the north, 65 ± 6 km ($T_n = 1.10 \pm 0.1$) for the center, and 67 ± 5 km ($T_n = 1.01 \pm 0.1$) for the south. By increasing the pre-deformation AP thickness to 40 km in the variable thickness model, in situ shortening was able to develop modern AP thicknesses by 0 Ma. Distributing the total predicted excess volume over the western margin of the plateau predicts a 48 km thick crust in the WC, ~20 km less than modern (Fig. 3). The thickness discrepancy could be explained by magmatic addition, but would require a ~30% contribution to the total crustal volume at the arc. Increases in initial SA thickness did not volumetrically compensate for the lower initial EC thickness compared to the uniform model. This suggests that the crustal budget is most sensitive to assumed initial EC thickness, likely due to the fact that it is where the greatest shortening magnitudes are accommodated. The excess crustal volume in the variable thickness model is ~40% lower than the 40 km thickness model and 42% greater than the 35 km thickness model. Consequently, the crustal thickening history predicted by the variable initial thickness model falls within the range defined by the 35 km and 40 km uniform thickness models.

A.3. Variable thickness model implications

In the variable thickness model, predicted northern EC excess at 20 Ma can accommodate a ≤6 km loss of lower crust, but EC volume deficits to the east may argue against sufficient regional thickening for a removal event (Fig. 7B). Material transfer after 15 Ma from the SA to the EC is sufficient to compensate for early, localized lower crustal loss and allow for a second ~7 km removal event but only after 5 Ma. Given the lower final excess volume in the variable thickness model, removing crust in two phases limits the possible volume contribution to the WC to ~3 km per unit area, predicting a mean thickness of 43 km.

Appendix B

B.1. Model uncertainty

Determining standardized uncertainties in the crustal thickness model is extremely complex due to the array of data used to reconstruct the map-view displacement field (Eichelberger and McQuarrie, 2015). As yet, there is no rigorous method for propagating uncertainties from various thermochronologic dating systems, paleomagnetic rotations, and shortening estimates into a meaningful reconstruction where the model variance reflects a range of geologically plausible solutions. However, we can investigate the effects of modifying the displacement field within a geologically permissible range to determine the influence on predicted crustal thickness. This approach does not provide standardized uncertainty estimates, but it further establishes the range of possible model results and is consistent with our approach of testing a range of initial crustal thickness (another substantial uncertainty in this study).

A fundamental requirement of any map-view reconstruction is that the displacement vectors for each structure must be kinematically compatible with surrounding regions and maintain strain compatibility (no overlapping displacement paths). Strain compatibility is assessed in a map-view reconstruction by the extent to which the displacement paths result in overlaps, indicating regions of strain incompatibility. In the original map-view reconstruction multiple scenarios were tested that explored the implications of varying poorly constrained kinematic parameters, such as out-of-plane displacements that are not quantified by shortening estimates from balanced cross sections (namely rotations and translations along structural trends). The reconstruction that honored the available constraints and produced minimal overlap was taken to reflect the "geologic best-fit". While accounting for out-of-plane displacements is necessary to accurately restore deformation in the central Andes (Kley, 1999), it results in higher overall shortening magnitudes than estimated by balanced cross sections (Arriagada et al., 2008; Eichelberger and McQuarrie, 2015). As a result, the displacement field used here records greater map-view area change than a reconstruction constrained exclusively by lower shortening estimates from balanced cross sections. If we take the cross section shortening estimates as the low end of permissible displacement, the resulting displacement field may not maintain strain compatibility, but it does provide a low-end estimate of crustal thickening.

B.2. Minimum shortening crustal thickness predictions

Since reducing the model displacement decreases the overall area change and predicted crustal volume, we compare the effects of low-end shortening estimates to the 35 km initial crustal thickness model. The difference in volume was calculated from the change in mesh area (Fig. 2B) for the EC, IA and SA based on the difference between map-view (best-fit displacement field) and balanced cross section shortening (low-end displacement field) in each zone (see Table 2 in Eichelberger and McQuarrie, 2015). The north, center, and south designations used here incorporate multiple cross section shortening estimates (Fig. 2A, Table B.1), so the difference in modeled (M, Table B.1) and cross section shortening (C, Table B.1) shortening estimates ranges from 63 to 67 km for the northern EC, 68 to 22 km in the central EC, and <5 km in the southern EC. Only the central IA has a significant difference in shortening (37 km). Cross section SA shortening estimates are 24 km less than modeled estimates in the north, 19 km in the center, and 22–16 km in the south. The total change in restored mesh area and crustal volume relative to the 35 km thickness model is −20% in the north, −8% in the center, and −3% change in the south (Table B.1). By 20 Ma (end of EC deformation), average predicted crustal thicknesses are at ~60% of modern in the northern EC ($T_n = 0.6 \pm 0.15$), ~75% modern in the central EC ($T_n = 0.77 \pm 0.10$), and 75% modern in the southern EC ($T_n = 0.75 \pm 0.12$). Comparatively, the 35 km model using the best-fit displacement field predicts >85% modern thickness in the north (Fig. 6A) and similar results to the low-end displacement field for the south. This is because the difference between map view and cross section displacement is greatest in the northern EC due to increased magnitudes of out of plane (strike-slip) displacement. Predicted thicknesses from the low-end displacement field at 0 Ma are still below modern in the north EC ($T_n = 0.75 \pm 0.2$) but have ~10% excess in the central ($T_n = 1.12 \pm 0.15$) and south EC ($T_n = 1.09 \pm 0.1$). Regionally, the net excess in the center and south

Table B.1
Table of difference in shortening magnitudes between cross section estimates (Transects 1–5 in Fig. 2A). The decrease in model area and volume are based on using the cross section shortening estimates.

Model region	Transect	Shortening (km)		Shortening difference (km)	Restored area difference (km^2)	Restored volume difference (km^3)	
		C	M			35 km model	40 km model
SA							
North	1	66	90	−24	−8675	−807 625	−923 000
Central	2	71	90	−19	−4300	−251 125	−287 000
	3	86	105	−19			
South	4	67	83	−16	−5500	−10 500	−12 000
	5	78	100	−22			
IA							
North	1	48	50	−2	0	0	0
Central	2	39	37	2	−1475	−51 625	−59 000
	3	43	80	−37			
South	4	96	97	−1	−2275	−79 625	−91 000
	5	62	61	1			
EC							
North	1	123	190	−67	−23 075	−303 625	−347 000
Central	2	142	210	−68	−7175	−150 500	−172 000
	3	136	158	−22			
South	4	122	125	−3	−300	−192 500	−220 000
	5	95	100	−5			
				Total	−52 775	−1 847 125	−2 111 000

EC balances the volume deficit in the AP and north EC to within 1% of the total modern volume. Therefore, minimum displacement implies a crustal history where modern crustal thicknesses were only achieved in the last 5 Ma and suggests material loss by removal or lower crustal flow was unlikely. A 40 km initial crustal thickness with the low-end displacement field predicts a 15% volume excess over modern at 0 Ma, comparable to results from the 35 km thickness model using the best-fit displacement field (12%; Figs. 7, 8).

In summary, crustal thickening models using low-end shortening estimates from the Bolivian Andes produce similar results to models with higher map-view displacements if initial crustal thicknesses are greater than 35 km. The minimum possible displacements from balanced cross sections only predict excess crustal material if initial crustal thicknesses are greater than 35 km. If initial crustal thicknesses were 35 km or less, low-end displacement estimates predict a crustal volume balance within the region but do not allow for material loss. These results are consistent with modeling by Hindle et al. (2005) that accounted for modern crustal thicknesses using lower (but incomplete) shortening estimates, similar rotations (∼250 km, ±10°; Kley, 1999), and a 40 km thick crust.

Appendix C. Supplementary material

Supplementary material related to this article can be found online at http://dx.doi.org/10.1016/j.epsl.2015.06.035.

References

Allmendinger, R.W., Smalley Jr., R., Bevis, M., Caprio, H., Brooks, B., 2005. Bending the Bolivian orocline in real time. Geology 33, 905–908. http://dx.doi.org/10.1130/G21779.1.

Arriagada, C., Roperch, P., Mpodozis, C., Fernandez, R., 2006. Paleomagnetism and tectonics of the southern Atacama Desert (25–28°S), northern Chile. Tectonics 25, TC4001. http://dx.doi.org/10.1029/2005TC001923.

Arriagada, C., Roperch, P., Mpodozis, C., Cobbold, P.R., 2008. Paleogene building of the Bolivian Orocline: tectonic restoration of the central Andes in 2-D map view. Tectonics 27, TC6014. http://dx.doi.org/10.1029/2008TC002269.

Baby, P., Moretti, I., Guillier, B., Limachi, R., Mendez, E., Oller, J., Specht, M., 1995. Petroleum system of the northern and central Bolivian sub-Andean zone. In: Tankard, A.J., Suárez Soruco, R., Welsink, H.J. (Eds.), Petroleum Basins of South America. In: AAPG Mem., vol. 62, pp. 445–458.

Barnes, J.B., Ehlers, T.A., 2009. End member models for Andean Plateau uplift. Earth-Sci. Rev. 97, 117–144. http://dx.doi.org/10.1016/j.earscirev.2009.08.003.

Barnes, J.B., Ehlers, T.A., McQuarrie, N., O'Sullivan, P.B., Pelletier, J.D., 2006. Eocene to recent variations in erosion across the central Andean fold-thrust belt, northern Bolivia; implications for plateau evolution. Earth Planet. Sci. Lett. 248, 118–133. http://dx.doi.org/10.1016/j.epsl.2006.05.018.

Beck, S.L., Zandt, G., 2002. The nature of orogenic crust in the central Andes. J. Geophys. Res. 107 (B10), 2230. http://dx.doi.org/10.1029/2000JB000124.

Beck, S.L., et al., 1994. Across the Andes and along the Altiplano: a passive seismic experiment. IRIS Newsl. XIII (3), 1–3.

Beck, S.L., Zandt, G., Myers, S.C., Wallace, T.C., Silver, P.G., Drake, L., 1996. Crustal-thickness variations in the central Andes. Geology 24, 407–410.

Dewey, J.F., Lamb, S.H., 1992. Active tectonics of the Andes. In: Oliver, R.A., Vatin-Pérignon, N., Laubacher, G. (Eds.), Andean Geodynamics. Tectonophysics 205, 79–95.

Dorbath, C., Granet, M., 1996. Local earthquake tomography of the Altiplano and Eastern Cordillera of northern Bolivia. Tectonophysics 259, 117–136.

Dorbath, C., Granet, M., Poupinet, G., Martinez, C., 1993. A teleseismic study of the Altiplano and the Eastern Cordillera in northern Bolivia: new constraints on a lithospheric model. J. Geophys. Res. 98, 9825–9844.

Dunn, J.F., Hartshorn, K.G., Hartshorn, P.W., 1995. Structural styles and hydrocarbon potential of the Subandean thrust belt of southern Bolivia. In: Tankard, A.J., Suarez, R., Welsink, H.J. (Eds.), Petroleum Basins of South America. In: AAPG Mem., vol. 62, pp. 523–543.

Eichelberger, N., McQuarrie, N., 2015. Kinematic reconstruction of the Bolivian orocline. Geosphere 11 (2). http://dx.doi.org/10.1130/GES01064.1.

Eichelberger, N., McQuarrie, N., Ehlers, T.A., Enkelmann, E., Barnes, J.B., Lease, R.O., 2013. New constraints on the chronology, magnitude, and distribution of deformation within the central Andean orocline. Tectonics 32, 1–22. http://dx.doi.org/10.1002/tect.20073.

Elger, K., Oncken, O., Glodny, J., 2005. Plateau-style accumulation of deformation; southern Altiplano. Tectonics 24, TC4020. http://dx.doi.org/10.1029/2004TC001675.

England, P., Houseman, G., 1988. The mechanics of the Tibetan plateau. Philos. Trans. R. Soc. Lond. A 327, 379–413.

Garzione, C.N., Auerbach, D.J., Smith, J.J.S., Rosario, J.J., Passey, B.H., Jordan, T.E., Eiler, J.M., 2014. Clumped isotope evidence for diachronous surface cooling of the Altiplano and pulsed surface uplift of the Central Andes. Earth Planet. Sci. Lett. 393, 173–181. http://dx.doi.org/10.1016/j.epsl.2014.02.029.

Garzione, C.N., Hoke, G.D., Libarkin, J.C., Withers, S., MacFadden, B.J., Eiler, J.M., Ghosh, P., Mulch, A., 2008. Rise of the Andes. Science 320, 1304–1307. http://dx.doi.org/10.1126/science.1148615.

Garzione, C.N., Molnar, P., Libarkin, J.C., MacFadden, B.J., 2006. Rapid late Miocene rise of the Bolivian Altiplano: evidence for removal of mantle lithosphere. Earth Planet. Sci. Lett. 241, 543–556.

Ghosh, P., Garzione, C.N., Eiler, J.M., 2006. Rapid uplift of the Altiplano revealed through ^{13}C–^{18}O bonds in paleosol carbonates. Science 311, 511–515. http://dx.doi.org/10.1126/science.1119365.

Gotberg, N., McQuarrie, N., Caillaux, V.C., 2010. Comparison of crustal thickening budget and shortening estimates in southern Peru (12–14°S); implications for

mass balance and rotations in the “Bolivian orocline”. Geol. Soc. Am. Bull. 122, 727–742. http://dx.doi.org/10.1130/B26477.1.
Hindle, D., Kley, J., Oncken, O., Sobolev, S., 2005. Crustal balance and crustal flux from shortening estimates in the Central Andes. Earth Planet. Sci. Lett. 230, 113–124. http://dx.doi.org/10.1016/j.epsl.2004.11.004.
Hoke, G.D., Garzione, C.N., 2008. Paleosurfaces, paleoelevation, and the mechanisms for the late Miocene topographic development of the Altiplano plateau. Earth Planet. Sci. Lett. 271, 192–201. http://dx.doi.org/10.1016/j.epsl.2008.04.008.
Horton, B.K., 2005. Revised deformation history of the Central Andes; inferences from Cenozoic foredeep and intermontane basins of the Eastern Cordillera, Bolivia. Tectonics 24, TC3011. http://dx.doi.org/10.1029/2003TC001619.
Husson, L., Sempere, T., 2003. Thickening the Altiplano crust by gravity-driven crustal channel flow. Geophys. Res. Lett. 30, 1243. http://dx.doi.org/10.1029/2002GL016877.
Isacks, B.L., 1988. Uplift of the Central Andean Plateau and bending of the Bolivian orocline. J. Geophys. Res. 93, 3211–3231. http://dx.doi.org/10.1029/JB093iB04p03211.
Kay, R.W., Kay, S.M., 1993. Delamination and delamination magmatism. Tectonophysics 219, 177–189.
Kley, J., 1996. Transition from basement-involved to thin-skinned thrusting in the Cordillera Oriental of southern Bolivia. Tectonics 15, 763–775.
Kley, J., 1999. Geologic and geometric constraints on a kinematic model of the Bolivian orocline. J. South Am. Earth Sci. 12, 221–235.
Kley, J., Monaldi, C.R., 1998. Tectonic shortening and crustal thickness in the Central Andes: how good is the correlation? Geology 26, 723–726.
Lamb, S., 2011. Did shortening in thick crust cause rapid Late Cenozoic uplift in the northern Bolivian Andes? J. Geol. Soc. 168, 1079–1092. http://dx.doi.org/10.1144/0016-76492001-008.
Lamb, S., Hoke, L., 1997. Origin of the high plateau in the Central Andes, Bolivia, South America. Tectonics 16, 623–649. http://dx.doi.org/10.1029/97TC00495.
Laubscher, H.P., 1965. Ein kinematisches modell der Jurafaltung. Eclogae Geol. Helv. 58, 232–318.
Leier, A.L., McQuarrie, N., Garzione, C., Eiler, J., 2013. Stable isotope evidence for multiple pulses of rapid surface uplift in the Central Andes, Bolivia. Earth Planet. Sci. Lett. 371–372, 49–58.
Lyon-Caen, H., Molnar, P., Suarez, G., 1985. Gravity anomalies and flexure of the Brazilian shield beneath the Bolivian Andes. Earth Planet. Sci. Lett. 75, 81–92.
McQuarrie, N., 2002. The kinematic history of the central Andean fold-thrust belt, Bolivia; implications for building a high plateau. Geol. Soc. Am. Bull. 114, 950–963. http://dx.doi.org/10.1130/00167606(2002)114<0950:TKHOTC>2.0.CO;2.
McQuarrie, N., Wernicke, B.P., 2005. An animated tectonic reconstruction of southwestern North America since 36 Ma. Geosphere 1, 147–172. http://dx.doi.org/10.1130/GES00016.1.
McQuarrie, N., Barnes, J.B., Ehlers, T.A., 2008. Geometric, kinematic, and erosional history of the central Andean Plateau, Bolivia (15–17°S). Tectonics 27, TC3007. http://dx.doi.org/10.1029/2006TC002054.
Müller, J.P., Kley, J., Jacobshagen, V., 2002. Structure and Cenozoic kinematics of the Eastern Cordillera, southern Bolivia. Tectonics 21, 1037. http://dx.doi.org/10.1029/2001TC001340.
Myers, S., Beck, S., Zandt, G., Wallace, T., 1998. Lithospheric-scale structure across the Bolivian Andes from tomographic images of velocity and attenuation for P and S waves. J. Geophys. Res. 103, 21233–21252.
Pope, D.C., Willett, S.D., 1998. Thermal-mechanical model for crustal thickening in the central Andes driven by ablative subduction. Geology 26, 511–514.
Roeder, D., Chamberlain, R.L., 1995. Structural geology of sub-Andean fold and thrust belt in northwestern Bolivia. In: Tankard, A.J., Suàrez Soruco, R., Welsink, H.J. (Eds.), Petroleum Basins of South America. In: AAPG Mem., vol. 62, pp. 459–479.
Roperch, P., Sempere, T., Macedo, O., Arriagada, C., Fornari, M., Tapia, C., Garcia, M., Laj, C., 2006. Counterclockwise rotation of late Eocene–Oligocene fore-arc deposits in southern Peru and its significance for oroclinal bending in the central Andes. Tectonics 25, TC3010. http://dx.doi.org/10.1029/2005TC001882.
Sempere, T., 1995. Phanerozoic evolution of Bolivia and adjacent regions. In: Tankard, A.J., Suàrez Soruco, R., Welsink, H.J. (Eds.), Petroleum Basins of South America. In: AAPG Mem., vol. 62, pp. 207–230.
Swenson, J., Beck, S., Zandt, G., 2000. Crustal structure of the Altiplano from broadband regional waveform modeling: implications for the composition of thick continental crust. J. Geophys. Res. 105, 607–621.
Tao, W.C., O'Connell, R.J., 1992. Ablative subduction: a two-sided alternative to the conventional subduction model. J. Geophys. Res. 97, 8877–8904.
Tassara, A., Götze, H.-J., Schmidt, S., Hackney, R., 2006. Three-dimensional density model of the Nazca plate and the Andean continental margin. J. Geophys. Res. 111, B09404. http://dx.doi.org/10.1029/2005JB003976.
Turcotte, D.L., Schubert, G., 2002. Geodynamics. Cambridge University Press, Cambridge, UK, 456 pp.
Watts, A.B., Lamb, S.H., Fairhead, J.D., Dewey, J.F., 1995. Lithospheric flexure and bending of the Central Andes. Earth Planet. Sci. Lett. 134, 9–21.
Welsink, H.J., Franco, A., Oviedo, C., 1995. Andean and pre-Andean deformation, Boomerang Hills area, Bolivia. In: Tankard, A.J., Suàrez Soruco, R., Welsink, H.J. (Eds.), Petroleum Basins of South America. In: AAPG Mem., vol. 62, pp. 481–499.
Whitman, D., Isacks, B.L., Kay, S.M., 1996. Lithospheric structure and along-strike segmentation of the Central Andean Plateau: seismic Q, magmatism, flexure, topography and tectonics. Tectonophysics 259, 29–40.
Yang, Y., Liu, M., Stein, S., 2003. A 3-D geodynamic model of lateral crustal flow during Andean mountain building. Geophys. Res. Lett. 30, 2093. http://dx.doi.org/10.1029/2003GL018308.
Yuan, X., Sobolev, S., Kind, R., 2002. Moho topography in the central Andes and its geodynamic implications. Earth Planet. Sci. Lett. 199, 389–402.
Zandt, G., Beck, S., Ruppert, S., Ammon, C., Rock, D., Minaya, E., Wallace, T., Silver, P., 1996. Anomalous crust of the Bolivian Altiplano, central Andes: constraints from broadband regional seismic waveforms. Geophys. Res. Lett. 23, 1159–1162.